

# UC Berkeley

## UC Berkeley Previously Published Works

### Title

HOx chemistry during INTEX-A 2004: Observation, model calculation, and comparison with previous studies

### Permalink

<https://escholarship.org/uc/item/0fw1k60r>

### Journal

Journal of Geophysical Research Atmospheres, 113(5)

### ISSN

0148-0227

### Authors

Ren, X  
Olson, JR  
Crawford, JH  
[et al.](#)

### Publication Date

2008-03-16

### DOI

10.1029/2007JD009166

### Copyright Information

This work is made available under the terms of a Creative Commons Attribution License, available at <https://creativecommons.org/licenses/by/4.0/>

Peer reviewed

## HO<sub>x</sub> chemistry during INTEX-A 2004: Observation, model calculation, and comparison with previous studies

Xinrong Ren,<sup>1,2</sup> Jennifer R. Olson,<sup>3</sup> James H. Crawford,<sup>3</sup> William H. Brune,<sup>1</sup> Jingqiu Mao,<sup>1</sup> Robert B. Long,<sup>1</sup> Zhong Chen,<sup>1</sup> Gao Chen,<sup>3</sup> Melody A. Avery,<sup>3</sup> Glen W. Sachse,<sup>3</sup> John D. Barrick,<sup>3</sup> Glenn S. Diskin,<sup>3</sup> L. Greg Huey,<sup>4</sup> Alan Fried,<sup>5</sup> Ronald C. Cohen,<sup>6</sup> Brian Heikes,<sup>7</sup> Paul O. Wennberg,<sup>8</sup> Hanwant B. Singh,<sup>9</sup> Donald R. Blake,<sup>10</sup> and Richard E. Shetter<sup>11</sup>

Received 13 July 2007; revised 24 October 2007; accepted 18 December 2007; published 8 March 2008.

[1] OH and HO<sub>2</sub> were measured with the Airborne Tropospheric Hydrogen Oxides Sensor (ATHOS) as part of a large measurement suite from the NASA DC-8 aircraft during the Intercontinental Chemical Transport Experiment-A (INTEX-A). This mission, which was conducted mainly over North America and the western Atlantic Ocean in summer 2004, was an excellent test of atmospheric oxidation chemistry. The HO<sub>x</sub> results from INTEX-A are compared to those from previous campaigns and to results for other related measurements from INTEX-A. Throughout the troposphere, observed OH was generally 0.95 of modeled OH; below 8 km, observed HO<sub>2</sub> was generally 1.20 of modeled HO<sub>2</sub>. This observed-to-modeled comparison is similar to that for TRACE-P, another midlatitude study for which the median observed-to-modeled ratio was 1.08 for OH and 1.34 for HO<sub>2</sub>, and to that for PEM-TB, a tropical study for which the median observed-to-modeled ratio was 1.17 for OH and 0.97 for HO<sub>2</sub>. HO<sub>2</sub> behavior above 8 km was markedly different. The observed-to-modeled HO<sub>2</sub> ratio increased from ~1.2 at 8 km to ~3 at 11 km with the observed-to-modeled ratio correlating with NO. Above 8 km, the observed-to-modeled HO<sub>2</sub> and observed NO were both considerably greater than observations from previous campaigns. In addition, the observed-to-modeled HO<sub>2</sub>/OH, which is sensitive to cycling reactions between OH and HO<sub>2</sub>, increased from ~1.5 at 8 km to almost 3.5 at 11 km. These discrepancies suggest a large unknown HO<sub>x</sub> source and additional reactants that cycle HO<sub>x</sub> from OH to HO<sub>2</sub>. In the continental planetary boundary layer, the observed-to-modeled OH ratio increased from 1 when isoprene was less than 0.1 ppbv to over 4 when isoprene was greater than 2 ppbv, suggesting that forests throughout the United States are emitting unknown HO<sub>x</sub> sources. Progress in resolving these discrepancies requires a focused research activity devoted to further examination of possible unknown OH sinks and HO<sub>x</sub> sources.

**Citation:** Ren, X., et al. (2008), HO<sub>x</sub> chemistry during INTEX-A 2004: Observation, model calculation, and comparison with previous studies, *J. Geophys. Res.*, 113, D05310, doi:10.1029/2007JD009166.

### 1. Introduction

[2] Oxidation chemistry cleanses the atmosphere of chemical emissions from Earth's surface, establishes the

global ozone balance, and influences climate change. It is dominated by the hydroxyl radical, OH, but also involves the hydroperoxyl radical, HO<sub>2</sub>. OH and HO<sub>2</sub>, together called HO<sub>x</sub>, are highly reactive atmospheric constituents that have a large impact on the atmospheric chemistry by

<sup>1</sup>Department of Meteorology, Pennsylvania State University, University Park, Pennsylvania, USA.

<sup>2</sup>Now at Rosenstiel School of Marine and Atmospheric Sciences, University of Miami, Miami, Florida, USA.

<sup>3</sup>Science Directorate, NASA Langley Research Center, Hampton, Virginia, USA.

<sup>4</sup>School of Earth and Atmospheric Sciences, Georgia Institute of Technology, Atlanta, Georgia, USA.

<sup>5</sup>Earth Observing Laboratory, National Center for Atmospheric Research, Boulder, Colorado, USA.

<sup>6</sup>Department of Chemistry and Department of Earth and Planetary Science, University of California, Berkeley, California, USA.

<sup>7</sup>Graduate School of Oceanography, University of Rhode Island, Narragansett, Rhode Island, USA.

<sup>8</sup>Division of Engineering and Applied Sciences, California Institute of Technology, Pasadena, California, USA.

<sup>9</sup>NASA Ames Research Center, Moffett Field, California, USA.

<sup>10</sup>Department of Chemistry, University of California, Irvine, California, USA.

<sup>11</sup>National Suborbital Education and Research Center, University of North Dakota, Grand Forks, North Dakota, USA.

influencing the removal of gases emitted into the atmosphere and the production of ozone and ultrafine aerosol particles.

[3] The basics of HO<sub>x</sub> photochemistry have frequently been described [see, e.g., *Jaeglé et al.*, 2000]. The abundance of OH and HO<sub>2</sub> is primarily influenced by the HO<sub>x</sub> production rate, the amount of NO<sub>x</sub> (NO<sub>x</sub> = NO + NO<sub>2</sub>), and to some extent the types of hydrocarbons [*Jaeglé et al.*, 2000; *McKeen et al.*, 1997; *Singh et al.*, 1995, 2003]. In polar regions during springtime, halogen chemistry can influence HO<sub>x</sub> and the HO<sub>2</sub>/OH ratio in both the marine boundary layer [*Bloss et al.*, 2007] and the stratosphere [*Hanisco et al.*, 2002].

[4] HO<sub>x</sub> has a number of sources: photolysis of ozone (O<sub>3</sub>) followed by a reaction of O(<sup>1</sup>D) with H<sub>2</sub>O, photolysis of formaldehyde (HCHO), nitrous acid (HONO), hydrogen peroxide (H<sub>2</sub>O<sub>2</sub>), methylhydroperoxide (CH<sub>3</sub>OOH), and acetone (CH<sub>3</sub>C(O)CH<sub>3</sub>), as well as reactions between O<sub>3</sub> and alkenes. Its destruction is thought to be controlled by the relatively few type reactions: HO<sub>2</sub> + HO<sub>2</sub>, HO<sub>2</sub> + OH, HO<sub>2</sub> + RO<sub>2</sub>, and OH + NO<sub>2</sub>.

[5] The NO<sub>x</sub> abundance determines which reactions are the primary HO<sub>x</sub> loss. At low NO<sub>x</sub>, radical-radical reactions (particularly HO<sub>2</sub> + HO<sub>2</sub> and HO<sub>2</sub> + RO<sub>2</sub>) dominate the loss of HO<sub>x</sub>. As NO<sub>x</sub> increases, HO<sub>2</sub> + NO → OH + NO<sub>2</sub> shifts the partitioning of HO<sub>x</sub> toward OH so that the HO<sub>2</sub> + OH reaction begins to contribute significant to the loss. At high NO<sub>x</sub>, direct reaction of OH with NO<sub>2</sub> to form HNO<sub>3</sub> becomes the primary loss. As a result, for fixed HO<sub>x</sub> production (P(HO<sub>x</sub>)), OH first increases until NO<sub>x</sub> reaches a few ppbv and then decreases as a function of NO<sub>x</sub>, while HO<sub>2</sub> remains roughly unchanged until NO<sub>x</sub> reaches values for which OH + NO<sub>2</sub> + M → HNO<sub>3</sub> + M is the dominant loss and then decreases even faster than OH as NO<sub>x</sub> continues to increase. As P(HO<sub>x</sub>) increases, the peak OH is higher and shifted to greater NO<sub>x</sub> values [*McKeen et al.*, 1997]. Under high NO<sub>x</sub> conditions, HO<sub>x</sub> has a heightened sensitivity to HO<sub>x</sub> sources [*Olson et al.*, 2006]. Thus, uncertainties in observations and reaction kinetics of HO<sub>x</sub> precursors have a much more pronounced impact on modeled HO<sub>x</sub> at high NO<sub>x</sub> conditions compared to lower NO<sub>x</sub> conditions.

[6] Reactions of OH with carbon monoxide (CO) and volatile organic compounds (VOCs) lead to the formation of HO<sub>2</sub> and organic peroxy radicals (RO<sub>2</sub>). This conversion of OH is rapid. The inverse of the OH lifetime, the reaction frequency, which is usually called the OH reactivity, is typically 1 s<sup>-1</sup> in clean environments near the surface, about 0.2–0.4 s<sup>-1</sup> in the upper troposphere, and 5–100 s<sup>-1</sup> in polluted urban environments. At the same time, HO<sub>2</sub> reacts with NO, producing O<sub>3</sub>, or with O<sub>3</sub>, destroying O<sub>3</sub>, and in the process recreates OH. This cycle between OH and HO<sub>2</sub> is at times faster than the production and loss of HO<sub>x</sub>. The reaction of RO<sub>2</sub> and NO leads to the formation of HO<sub>2</sub> and NO<sub>2</sub>. The exact photochemistry that occurs depends mainly on the HO<sub>x</sub> production (P(HO<sub>x</sub>)), NO<sub>x</sub>, the OH reactivity, and the yield of HO<sub>2</sub> and RO<sub>2</sub> from hydrocarbon oxidation [*Kleinman et al.*, 2002]. Understanding HO<sub>x</sub> sources, sinks, and cycling is essential to develop predictive capability of pollution's influence on the atmosphere's oxidation capacity.

[7] The ratio of HO<sub>2</sub>/OH is an important indicator of the HO<sub>x</sub> cycling between OH and HO<sub>2</sub>. A steady state expres-

sion for HO<sub>2</sub>/OH comes from assuming that OH is in steady state:

$$\frac{[HO_2]}{[OH]} = \frac{k_{OH}}{(k_{NO+HO_2}[NO] + k_{O_3+HO_2}[O_3]) + P(OH)_{primary}/[HO_2]} \quad (1)$$

where P(OH)<sub>primary</sub> is the OH production rate from either photolysis of long-lived atmospheric constituents or from reactions of O<sub>3</sub> with alkenes; (k<sub>NO+HO<sub>2</sub></sub>[NO] + k<sub>O<sub>3</sub>+HO<sub>2</sub></sub>[O<sub>3</sub>]) represents the cycling reaction frequency of HO<sub>x</sub> from HO<sub>2</sub> to OH; and k<sub>OH</sub> is the OH reactivity with all OH reactants, whether they are HO<sub>x</sub> cycling or HO<sub>x</sub> terminating reactions. We use the definition for primary OH sources to be those that are independent of local HO<sub>x</sub> [*Jaeglé et al.*, 2001]. Typically the photolysis of O<sub>3</sub> followed by O(<sup>1</sup>D) + H<sub>2</sub>O is the most important OH primary source, although the photolysis of HONO, H<sub>2</sub>O<sub>2</sub>, and CH<sub>3</sub>OOH can also be important.

[8] For many atmospheric environments, the primary production, P(OH)<sub>primary</sub>, and the terminating OH reaction rates are much smaller than the rate of reactions that cycle HO<sub>x</sub> between OH and HO<sub>2</sub> and can be ignored. However, for the free troposphere between 2 km and 8 km in INTEx-A, the fraction of OH production by P(OH)<sub>primary</sub> is as often larger than OH production by HO<sub>x</sub> cycling, ranging from 0.1 to 0.9 of total OH production, and cannot be ignored.

[9] Because HO<sub>x</sub> photochemistry is sufficiently fast, comparisons with box models test the understanding of HO<sub>x</sub> photochemistry. While scatterplots of measurements and model calculations are useful, examining the ratio of observed-to-modeled OH and HO<sub>2</sub> as a function of important variables provides even more information. The analyses of airborne tropospheric HO<sub>x</sub> measurements from several different studies have been published [e.g., *Wennberg et al.*, 1998; *Crawford et al.*, 1999; *Brune et al.*, 1998, 1999; *Tan et al.*, 2001a; *Olson et al.*, 2004, 2006]. When all of the studies are taken together, we can reach the conclusion that HO<sub>x</sub> photochemistry is generally understood and the results from last several missions are generally consistent, but that important large differences remain for some environments and conditions.

[10] Although the current agreement between measured and modeled HO<sub>x</sub> is generally very good, there are specific environmental conditions where the agreement is weaker. Considering the critical role of HO<sub>x</sub> in the production of secondary pollutants and the role of OH in the troposphere's oxidation capacity, further investigation into the causes of these differences is crucial. Emerging from previous HO<sub>x</sub> studies are a set of conclusions: (1) HO<sub>2</sub>, and thus calculated ozone production, is greater than model predictions at larger NO values for many tower-based studies and some aircraft studies, even though this discrepancy has been almost eliminated for two previous aircraft studies by reanalyses that more fully account for HO<sub>x</sub> precursors and have updated reaction rate coefficients and products [*Olson et al.*, 2006]; (2) HO<sub>2</sub> and OH are larger than model predictions at high solar zenith angles, as in the Subsonic Assessment: Ozone and Nitrogen Oxide Experiment (SONEX) [*Brune et al.*, 1999], although the overtone photolysis of HO<sub>2</sub>NO<sub>2</sub> could partly explain the discrepancy

[Murphy *et al.*, 2004]; (3) the evidence for heterogeneous influence on HO<sub>x</sub> is still inconclusive, although some studies have provided evidence for significant removal in clouds [Olson *et al.*, 2006]; (4) even with highly constraining measurement suites, OH and HO<sub>2</sub> can be either significantly larger or smaller than model predictions in different environments and on different missions; whether this variation in agreement is due to unmeasured atmospheric constituents, instrumental drifts and changes, or differences in models, or a combination of all three, is not known; and (5) agreement of OH and HO<sub>2</sub> measured by different instruments has been inconsistent from comparison to comparison and for individual instrument in different environments [Eisele *et al.*, 2001, 2003; Ren *et al.*, 2003].

[11] This paper presents HO<sub>x</sub> observation results and a steady state modeling analysis of fast photochemistry using measurements made during the INTEX-A campaign. The HO<sub>x</sub> results from INTEX-A are compared to those from previous campaigns and to results for other related measurements from INTEX-A. Analyses of these comparisons provide the characteristics that uncertain or unknown chemistry must have in order to resolve discrepancies between measured and modeled HO<sub>x</sub> that were observed in INTEX-A.

## 2. Experiment and Model Description

### 2.1. OH and HO<sub>2</sub> Measurements

[12] The OH and HO<sub>2</sub> radicals were measured with the Penn State ATHOS (Aircraft Tropospheric Hydrogen Oxides Sensor). ATHOS detects OH and HO<sub>2</sub> with laser-induced fluorescence (LIF). The technique uses a pump-down technique often called the fluorescent assay by gas expansion (FAGE) originally developed by Hard *et al.* [1984]. A detailed description of the ATHOS instrument can be found elsewhere [Faloona *et al.*, 2004]; here an abbreviated description of ATHOS is given.

[13] The air sample is drawn into a low-pressure chamber through a pinhole inlet (1.5 mm) with a vacuum pump. The pressure of the detection chamber varied from 12 to 3 hPa from 0 to 12 km altitude. As the air passes through a laser beam, OH is excited by a spectrally narrowed laser with a pulse repetition rate of 3 kHz at one of several ro-vibronic transition lines near 308 nm ( $A^2\Sigma-X^2\Pi$ ,  $v' = 0 \leftarrow v'' = 0$ ). Collisional quenching of the excited state is slow enough at the chamber pressure that the weak OH fluorescence extends beyond the prompt scattering (Rayleigh and wall scattering) and is detected with a time-gated microchannel plate (MCP) detector. HO<sub>2</sub> is measured by reaction with NO followed by the LIF detection of OH. The OH and HO<sub>2</sub> detection axes are in series: OH is detected in the first axis and HO<sub>2</sub> in a second axis as reagent NO (>99%, Matheson, Twinsburg, OH, purified through Ascarite) is added to the flow between the two axes. The OH fluorescence signal is detected 60 ns after the laser pulse has cleared in the detection cells and is recorded every 0.2 s. The laser wavelength is tuned on and off resonance with an OH transition every 10 s, resulting in a measurement time resolution of 20 s. The OH fluorescence signal is the difference between on-resonance and off-resonance signals.

[14] The instrument was calibrated both in the laboratory and during the field campaign. Different sizes of pinholes

were used in the calibration to produce different detection cell pressures. Monitoring laser power, Rayleigh scattering, and laser line width maintained this calibration in flight [Faloona *et al.*, 2004]. For the calibration, OH and HO<sub>2</sub> were produced through water vapor photolysis by 185 nm light. Absolute OH and HO<sub>2</sub> mixing ratios were calculated by knowing the 185 nm flux, which is determined with a Cs-I phototube referenced to a NIST-calibrated photomultiplier tube, the H<sub>2</sub>O absorption cross section, the H<sub>2</sub>O mixing ratio, and the exposure time of the H<sub>2</sub>O to the 185 nm light. The absolute uncertainty is estimated to be a factor of 1.32 for both OH and HO<sub>2</sub>, at the 2 $\sigma$  confidence level. The uncertainty in measured HO<sub>2</sub>/OH ratios is less, about  $\pm 15\%$  at the 2 $\sigma$  confidence level, as determined from the precision of repeated simultaneous OH and HO<sub>2</sub> calibrations combined with estimated uncertainties of known factors affecting the relative OH and HO<sub>2</sub> measurements. The 2 $\sigma$  precisions for a 1-min integration time during this campaign were about 0.01 pptv for OH and 0.1 pptv for HO<sub>2</sub>. Further details about the calibration process may be found elsewhere [Faloona *et al.*, 2004].

[15] Recently we revised our values for OH and HO<sub>2</sub> for the NASA missions TRACE-P, INTEX-A, and INTEX-B because of a problem with the ATHOS absolute calibration. The problem was related to an error in the calibration of our primary standard: a photomultiplier tube (PMT), which we use to measure the photon flux of a mercury lamp in our OH generator. The revised numbers are factor of 1.64 higher. Missions earlier than TRACE-P were unaffected. The conclusions of a few papers already published concerning these missions will need to be revisited to see if the ATHOS calibration change affects them.

### 2.2. Other Measurements on the DC-8

[16] The payload of the DC-8 and the measured chemical species and parameters are briefly described by Singh *et al.* [2006]. A large suite of atmospheric constituents were measured in INTEX-A, including CO, O<sub>3</sub>, H<sub>2</sub>O, reactive nitrogen (NO, NO<sub>2</sub>, HNO<sub>3</sub>, HO<sub>2</sub>NO<sub>2</sub>, PAN), more than 50 VOCs and oxygenated VOCs (OVOCs), and important HO<sub>x</sub> precursors such as peroxides (H<sub>2</sub>O<sub>2</sub> and CH<sub>3</sub>OOH) and aldehydes (HCHO and acetaldehyde). Spectral radiometers allowed direct measurement of actinic flux used to derive key photolysis frequencies.

[17] The measurements of NO<sub>2</sub> were made with laser-induced fluorescence [Thornton *et al.*, 2000] and measurements of NO were made with a TECO Model 42C NO-NO<sub>x</sub> analyzer run in an NO only mode, which had a precision of 50 pptv with 1-min time integration. Because of this large NO limit of detection, concentrations of NO were predicted using the steady state model and measured NO<sub>2</sub>. A linear regression of the NO obtained from measurements and the model is the equation:  $\text{NO}_{\text{modeled}} = 0.92 \times \text{NO}_{\text{measured}} - 16$  pptv, with  $R^2 = 0.76$  and where,  $\text{NO}_{\text{modeled}}$  was calculated in the model using observed NO<sub>2</sub>, O<sub>3</sub>, NO<sub>2</sub> photolysis frequency, and modeled HO<sub>2</sub> and RO<sub>2</sub>. This agreement gives confidence that NO from the model, rather than measurements, can be used at low NO, where the NO measurement is noisy and may have a small offset, and at high NO, where NO obtained from measurements and from the model are in excellent agreement.



### 2.3. Model Description

[18] A zero-dimensional, time-dependent photochemical box model developed at NASA Langley Research Center was used to calculate OH, HO<sub>2</sub> and other reactive intermediates. The model has been described in detail in several previous studies [e.g., Crawford *et al.*, 1999; Olson *et al.*, 2004]. The modeling approach is based on the assumption of a diurnal steady state. For a suite of simultaneous measurements of input species at a given point in time, the model integrates to find a self-consistent diurnal cycle for the computed species based on constraining selected species to the measurements. Computed concentrations at the point in time of measurement are then used as the instantaneous model results. This approach ensures that all computed species are in equilibrium with the diurnal process, which is crucial for species with lifetimes too long for simple instantaneous steady state assumptions. For input, model calculations use observations from the 1-min merged data set available on the INTEX-A public data archive (<ftp://ftp-air.larc.nasa.gov/pub-air/INTEXA/>). The minimum set of input constraints includes observations of O<sub>3</sub>, CO, NO<sub>2</sub>, NMHC, acetone, methanol, temperature, H<sub>2</sub>O (dew/frost point), pressure, and photolysis frequencies. For this analysis, analyzed data were limited to solar zenith angles (SZA) between 0° and 85°.

[19] In addition to the required constraints described above, the model has the option to include additional constraints when measurements are available for hydrogen peroxide (H<sub>2</sub>O<sub>2</sub>), methyl hydrogen peroxide (CH<sub>3</sub>OOH), nitric acid (HNO<sub>3</sub>), and peroxy acetyl nitrate (PAN). If unavailable, these atmospheric constituents are calculated by the model based on diurnal steady state. While each of the H<sub>2</sub>O<sub>2</sub>, CH<sub>3</sub>OOH, HNO<sub>3</sub>, or PAN measurements were missing 20–35% of the measurement time, all of the H<sub>2</sub>O<sub>2</sub>, CH<sub>3</sub>OOH, HNO<sub>3</sub>, and PAN measurements were simultaneously missing less than 2% of the measurement time. Model calculations taking advantage of these additional constraints are referred to as “constrained.” All model results discussed in this paper are taken from the constrained model calculations unless explicitly stated otherwise. For the purpose of model-to-measurement comparisons, an unconstrained version was also run for which none of the additional constraints were exercised; that is, the peroxides, PAN, and HNO<sub>3</sub> were always predicted.

[20] Neither the unconstrained model nor the constrained model was constrained to the measured HCHO, just as was done for previous campaigns. Rather, HCHO is used as an additional species for which comparisons between the observations and model may provide insight into current knowledge of photochemical cycling. Evidence suggests that the differences in the observed and modeled HCHO do not significantly influence the comparisons between observed and modeled OH, HO<sub>2</sub>, and HO<sub>2</sub>/OH [Olson *et al.*, 2004; A. Fried *et al.*, Role of convection in redistributing formaldehyde to the upper troposphere over North America and the North Atlantic during the summer 2004 INTEX campaign, submitted to *Journal of Geophysical Research*, 2007].

[21] In order to maximize the number of points available for modeling, nonmethane hydrocarbons were interpolated between consecutive grab samples, which were collected throughout each flight at a frequency of every 4–5 min

during horizontal flight legs and every 1–2 min during ascents and descents. Similarly, acetone and methanol were interpolated between adjacent measurements to fill data gaps.

[22] As in previous studies, photolysis frequencies were based on spectroradiometer measurements [Shetter and Muller, 1999]. The diurnal profile for each photolysis frequency is based on clear-sky model calculations using a Discrete Ordinate Radiative Transfer (DISORT) eight-stream implementation of the NCAR Tropospheric Ultraviolet Visible (TUV) radiative transfer code [Madronich and Flocke, 1998]. The clear-sky diurnal variation from TUV is then normalized to measured photolysis frequencies at the time of observation. Unmeasured photolysis frequencies  $J[\text{NO}_3 + h\nu \rightarrow \text{NO} + \text{O}_2]$ ,  $J[\text{NO}_3 + h\nu \rightarrow \text{NO}_2 + \text{O}]$ , and  $J[\text{N}_2\text{O}_5 + h\nu \rightarrow \text{NO}_2 + \text{NO}_3]$  were first calculated for clear sky conditions and then corrected for ambient cloud conditions on the basis of the ratio of measured-to-calculated photolysis frequency of NO<sub>2</sub>.

[23] The uncertainties in the modeled OH and HO<sub>2</sub> are based on the combined uncertainties of the kinetic rate coefficients, the measured chemical concentrations, and the measured and calculated photolysis frequencies. The uncertainties in the model due to kinetic rate constant uncertainties were estimated with a Monte Carlo approach, as in, for example, the works by Thompson and Stewart [1991] or Carslaw *et al.* [1999]. The 2σ uncertainty was estimated to be ±59% for OH and ±53% for HO<sub>2</sub> in the upper troposphere (8–12 km), about ±40% for OH and 45% for HO<sub>2</sub> in the middle troposphere (2–8 km), and ±28% for OH and ±24% for HO<sub>2</sub> in the boundary layer, on the basis of median conditions observed for INTEX-A.

### 3. Observations, Model Results, and Comparisons

[24] During INTEX-A, the DC-8 encountered a variety of air masses. These include air masses that were influenced by anthropogenic pollution, biomass burning, convection, the stratosphere, and mixtures of these different types. These plumes are often distinguishable by their characteristic composition. Anthropogenic pollution contains high CO, anthropogenic hydrocarbons, and often water vapor. Biomass burning plumes can be distinguished from anthropogenic pollution by high HCN and acetonitrile. Convection plumes can be distinguished by high NO<sub>x</sub>/NO<sub>y</sub> ratios, water vapor, ultrafine particles, and O<sub>3</sub>. Stratosphere-influenced air can be defined as air having O<sub>3</sub> greater than ∼100 ppbv, CO less than ∼100 ppbv, water vapor less than 200 ppmv, and low hydrocarbon levels. The different composition of these air masses provides an excellent opportunity to examine HO<sub>x</sub> photochemistry for a range of conditions.

#### 3.1. HO<sub>x</sub> Observations and Comparison With the Model Calculations

[25] Altitude profiles of observed OH and HO<sub>2</sub> spanned from a few hundred meters above the surface to almost 12 km (Figure 1). Median OH was relatively constant at 0.25 pptv from altitudes near the surface to 6 km, but then increased with altitude above 6 km, achieving a maximum of about 0.86 pptv at 12 km. HO<sub>2</sub> decreased as the altitude increased, with a maximum median of ∼30 pptv near the

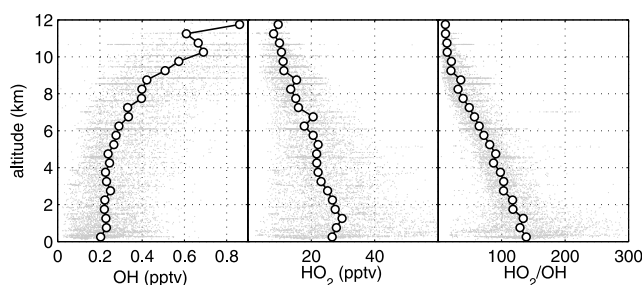


**Figure 1.** Observed OH and HO<sub>2</sub> mixing ratios and HO<sub>2</sub>/OH ratio as a function of altitude during INTEX-A. Small dots are the 1-min averaged data; the linked circles denote median values in 0.5 km altitude bins.

surface and a minimum median of  $\sim 8$  pptv at the highest altitude. The greatest HO<sub>2</sub>, almost 60 pptv, was observed just above the surface over the central United States. The median HO<sub>2</sub>/OH ratio dropped from 140 near the surface to 12 above 10 km, driven by both the decrease in HO<sub>2</sub> and the increase in OH with altitude. At low altitudes, the spread in HO<sub>2</sub>/OH is quite large, from 20 to 300, indicating a wide range of air composition there.

[26] Overall comparisons of observed and modeled OH and HO<sub>2</sub> show that on average observed OH and HO<sub>2</sub> generally agree with modeled OH and HO<sub>2</sub>. However, for less HO<sub>x</sub>, observed OH and HO<sub>2</sub> generally exceeded the modeled OH and HO<sub>2</sub> (Figure 2). Because less HO<sub>2</sub> was mostly observed at high altitudes, these plots suggest that the behavior of HO<sub>x</sub> should be investigated as a function of altitude.

[27] Detailed statistics characterize the behavior of the observed-to-modeled ratios as a function of altitude for OH, HO<sub>2</sub>, and HO<sub>2</sub>/OH (Table 1). The “% within  $\pm 32\%$ ” is the percentage of model values that are the same as the measured values to within the measurement  $2\sigma$  uncertainty of a factor of 1.32; the “% mod  $> \text{obs} \times 1.32$ ” is the percentage of model values greater than 1.32 times the observed values; and the “% mod  $< \text{obs}/1.32$ ” is the percentage of model values less than the observed values divided by 1.32. Although the model also has uncertainty, using the  $2\sigma$  measurement uncertainty provides a good indication of the differences between the observed and modeled values and where they are occurring.

[28] OH is well predicted by the model at all altitudes except in the boundary layer where OH is underpredicted, with roughly half of the modeled values falling within the  $2\sigma$  measurement uncertainty ( $\pm 32\%$ ) (Table 1 and Figure 3). For a smaller number of observations, OH is underpredicted in the continental boundary layer and in a few plumes at higher altitudes. The underprediction in the boundary layer correlates strongly with isoprene and will be discussed in detail later. HO<sub>2</sub> is generally well predicted below 8 km with a slight underprediction, but is significantly underpredicted above 8 km (Table 1 and Figure 4). Large underpredictions of HO<sub>2</sub> in the upper free troposphere above 8 km are highly correlated with NO and will be discussed in detail later.

[29] The HO<sub>2</sub>/OH ratio is generally well predicted throughout the troposphere (Table 1 and Figure 5). Below 8 km, the median observed-to-modeled ratio is less than 1.5. Median values of the HO<sub>2</sub>/OH observed-to-modeled ratio are biased slightly high because it tends to be slightly

underpredicted for HO<sub>2</sub>. Above 8 km, the large differences in the observed-to-modeled HO<sub>2</sub>/OH are driven more by the differences in observed-to-modeled HO<sub>2</sub> than they are in the differences between the observed-to-modeled OH.

[30] There are two possible explanations for the general observed and modeled agreement in some cases but not in others. The first explanation is that OH and HO<sub>2</sub> measurements are affected by large interferences in some environments. ATHOS has been extensively tested for interferences for both OH and HO<sub>2</sub> [Ren *et al.*, 2004]; no interference that could be responsible for these measurements has been found. A second explanation is that uncertainties or unknowns in the chemistry are responsible for at least some of the observed-to-modeled discrepancies. In the absence of evidence that the absolute calibration is not good to within the stated  $\pm 32\%$  at the  $2\sigma$  confidence level, we will assume that all the discrepancies are caused by uncertain or unknown chemistry and will at least characterize the effects of the unknown chemistry, even if we cannot identify it by name.

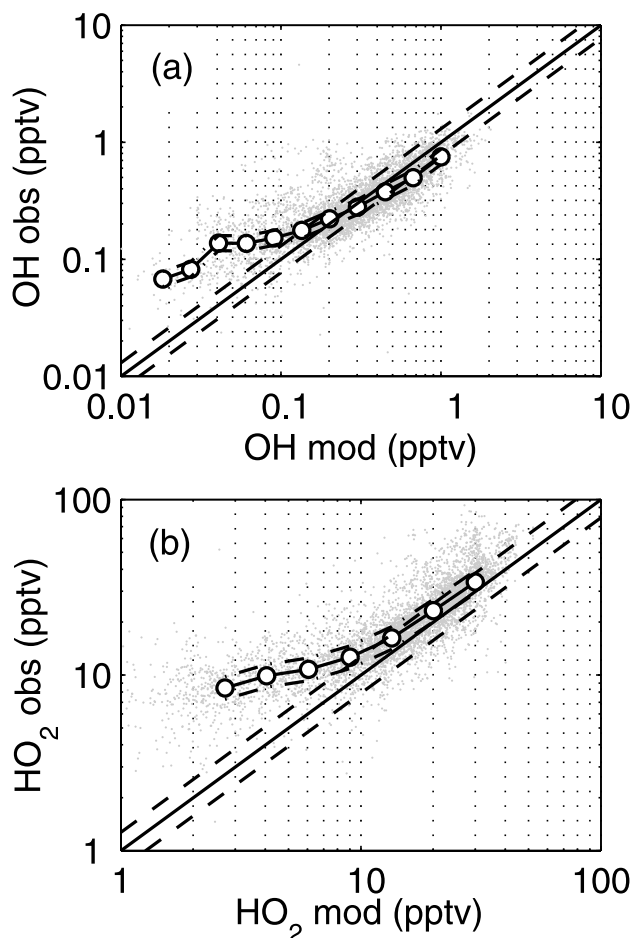


**Figure 2.** Comparison of observed and modeled (a) OH and (b) HO<sub>2</sub> in INTEX-A. The straight solid lines indicate the 1:1 lines, the dashed lines indicate the  $1\text{-}\sigma$  uncertainty in the model ( $\pm 30\%$  for OH and  $\pm 27\%$  for HO<sub>2</sub>, the maximum uncertainties estimated for the 8–12 km altitude range), the solid line with circles are the median values for the observations, and the dash-dotted lines are the  $1\text{-}\sigma$  uncertainty for the observations ( $\pm 16\%$ ).

**Table 1.** Statistics for HO<sub>x</sub> Observed-to-Modeled Ratios

|                                  | Overall     | 0–2 km      | 2–8 km      | 8–12 km     |
|----------------------------------|-------------|-------------|-------------|-------------|
| <i>OH Obs/Mod</i>                |             |             |             |             |
| Median (mean)                    | 0.95 (1.24) | 1.00 (1.54) | 0.92 (1.05) | 0.98 (1.25) |
| % within $\pm 32\%$              | 52%         | 47%         | 58%         | 50%         |
| % mod < obs/1.32 below $2\sigma$ | 23%         | 34%         | 16%         | 24%         |
| % mod > obs $\times 1.32$        | 25%         | 19%         | 26%         | 26%         |
| <i>HO<sub>2</sub> Obs/Mod</i>    |             |             |             |             |
| Median (mean)                    | 1.28 (2.87) | 1.37 (1.57) | 1.13 (2.10) | 2.05 (5.49) |
| % within $\pm 32\%$              | 50%         | 41%         | 74%         | 19%         |
| % mod < obs/1.32 below $2\sigma$ | 46%         | 56%         | 20%         | 79%         |
| % mod > obs $\times 1.32$        | 4%          | 3%          | 6%          | 2%          |
| <i>HO<sub>2</sub>/OH Obs/Mod</i> |             |             |             |             |
| Median (mean)                    | 1.33 (1.68) | 1.26 (1.26) | 1.20 (1.24) | 2.20 (2.88) |
| % within $\pm 32\%$              | 40%         | 40%         | 55%         | 13%         |
| % mod < obs/1.32 below $2\sigma$ | 50%         | 44%         | 36%         | 83%         |
| % mod > obs $\times 1.32$        | 10%         | 16%         | 9%          | 4%          |

### 3.2. Comparisons of Observed and Modeled HO<sub>x</sub> With Previous Studies

[31] ATHOS has measured OH and HO<sub>2</sub> during several recent field studies. The three most recent are the Pacific Exploratory Mission Tropics–B (PEM-TB) [Raper *et al.*, 2001], TRACE-P [Jacob *et al.*, 2003], and INTEX-A [Singh *et al.*, 2006]. PEM-TB was conducted in the tropical Pacific, usually in relatively clean air. In contrast, TRACE-P was conducted off the coast of Asia in air that was often quite polluted. Both occurred in spring and provide an interesting contrast to INTEX-A, which was conducted either over the continental US or over the Atlantic Ocean downwind of it in summer. Comparisons of these three studies are particularly compelling because ATHOS was used to measure OH and

HO<sub>2</sub> in all three and OH, HO<sub>2</sub>, and HCHO for several previous missions including PEM-TB and TRACE-P were recently recalculated using the same photochemistry and constraints as were used for INTEX-A [Olson *et al.*, 2006].

[32] The behavior of atmospheric constituents that interact with OH and HO<sub>2</sub> is quite different for the three studies (Figure 6). Carbon monoxide (CO) is similar for TRACE-P and INTEX-A, except at lower altitudes where Asian pollution observed during TRACE-P contained much more CO than North American pollution observed during INTEX-A. CO in both northern hemisphere studies are roughly twice that observed in PEM-TB. O<sub>3</sub> is similar for INTEX-A and TRACE-P up to  $\sim 8$  km, where O<sub>3</sub> in INTEX-A continues to increase. O<sub>3</sub> in PEM-TB is less than

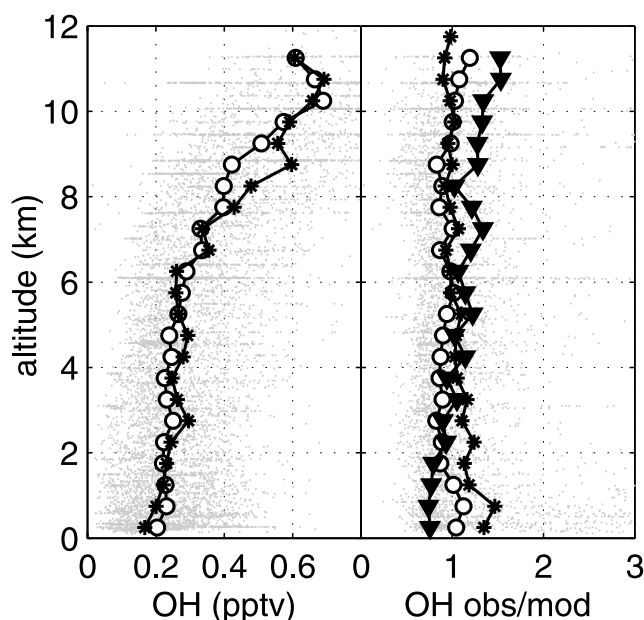


**Figure 3.** Comparison of the median vertical profiles of (left) measured (circles) and modeled (stars) OH in INTEX-A and (right) measured-to-modeled OH ratios in INTEX-A (circles), TRACE-P (stars) and PEM Tropics B (triangles). Individual INTEX-A 1-min measurements are shown (gray dots). The lines in the right diagram represent the median values of 1-min time-resolved obs/mod ratios.

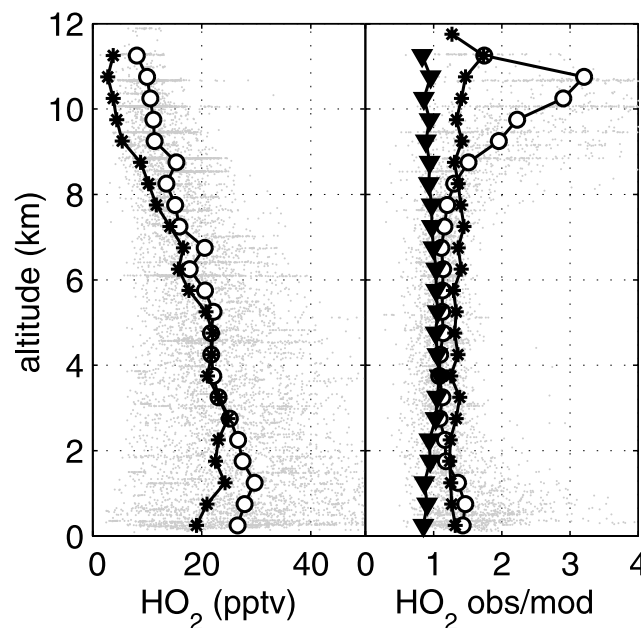


**Figure 4.** Comparison of the median vertical profiles of (left) measured (circles) and modeled (stars) HO<sub>2</sub> in INTEX-A and (right) measured-to-modeled HO<sub>2</sub> ratios in INTEX-A (circles), TRACE-P (stars) and PEM Tropics B (triangles). Individual INTEX-A 1-min measurements are shown (gray dots). The lines in the right diagram represent the median values of 1-min time-resolved obs/mod ratios.



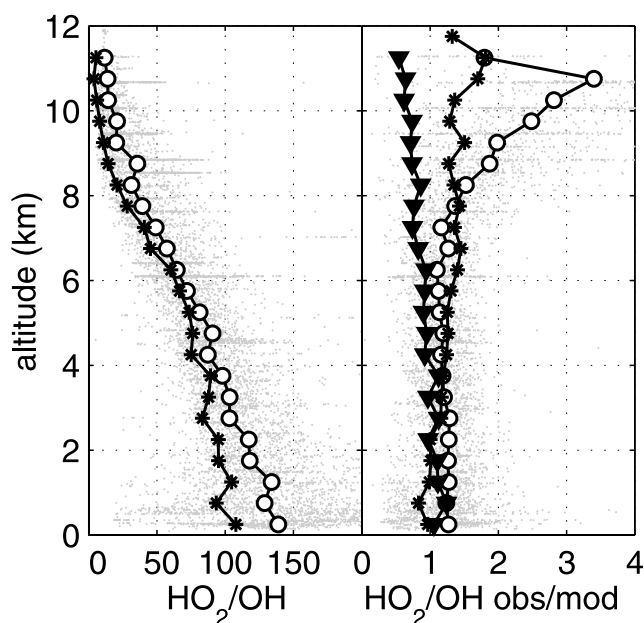


**Figure 5.** Comparison of the median vertical profiles of (left) measured (circles) and modeled (stars) HO<sub>2</sub>/OH in INTEX-A and (right) measured-to-modeled HO<sub>2</sub>/OH in INTEX-A (circles), TRACE-P (stars) and PEM Tropics B (triangles). Individual INTEX-A 1-min measurements are shown (gray dots). The lines in the right diagram represent the median values of 1-min time-resolved obs/mod ratios.

half these other two studies. The greatest differences were with NO<sub>x</sub>. Observed NO<sub>x</sub> was more than four to five times larger during INTEX-A than during TRACE-P and more than an order of magnitude larger than during PEM-TB. These differences are most pronounced above 8 km, where NO<sub>x</sub> during INTEX-A was sometimes more than 1.5 ppbv.

[33] The conditions among the three studies are quite different. It is therefore instructive to compare not only the absolute values of OH, HO<sub>2</sub>, and the HO<sub>2</sub>/OH ratio, but also the ratios of the measured-to-modeled OH, HO<sub>2</sub>, and HO<sub>2</sub>/OH ratio for the three studies. These are plotted as a function of the controlling environmental factors such as altitude (Figures 3, 4, and 5) and NO (Figure 7).

### 3.2.1. Comparison as a Function of Altitude

[34] As stated in section 2.1, the observed OH and HO<sub>2</sub> mixing ratios in INTEX-A and TRACE-P have been increased by a factor of 1.64 because of a calibration correction. The median observed-to-modeled OH ratio in INTEX-A is similar to that observed in TRACE-P (Figure 3). On the other hand, the median observed-to-modeled OH ratio in INTEX-A is different from that in PEM-Tropics B, where it was ~0.7 only below 1 km; above that, the median observed-to-modeled OH ratio increases monotonically to 1.3 at 12 km [Tan *et al.*, 2001a; Olson *et al.*, 2001].

[35] The observed-to-modeled HO<sub>2</sub> ratio has quite different behavior as a function of altitude in INTEX-A compared to that in either TRACE-P or PEM-TB (Figure 4). For altitudes between 2 km and below 8 km, the observed-to-modeled HO<sub>2</sub> ratio is similar for INTEX-A, TRACE-P and PEM-TB, all being around 1. In all three studies, the ratio changed little over this altitude range. The large increase in the observed-to-modeled HO<sub>2</sub> ratio above 8 km is quite different from either TRACE-P or PEM-TB. This difference is consistent with the substantially greater NO<sub>x</sub> observed above 8 km during INTEX-A than during the other two studies (Figure 6). For altitudes below 2 km, the observed-to-modeled HO<sub>2</sub> is about 1.5 for INTEX-A, 1.3 for TRACE-P, and 1.0 for PEM-TB.

[36] Enhanced NO<sub>x</sub> was also observed during SUCCESS (Subsonic aircraft; Contrails and Clouds Effect Special Study), both in and out of aircraft exhaust plumes. The ability to conclusively analyze the observations made in the exhaust plumes was limited by sampling with insufficient resolution to appropriately model nonlinear HO<sub>x</sub>-NO<sub>x</sub> interactions [Olson *et al.*, 2006]. For the SUCCESS observations not impacted directly by aircraft exhaust, a tendency for significant deviation between modeled and observed HO<sub>2</sub> remains [Brune *et al.*, 1998]. However, the lack of measurements of several potentially important HO<sub>x</sub> precursors limits what can be said with confidence about the underpredicted HO<sub>2</sub> that was observed during SUCCESS.

[37] Similar behavior was observed during TRACE-P, where a subset of the TRACE-P observations in stratospherically influenced air above 9 km near 35°N had an observed-to-modeled HO<sub>2</sub> ratio of 2.6 [Olson *et al.*, 2004].

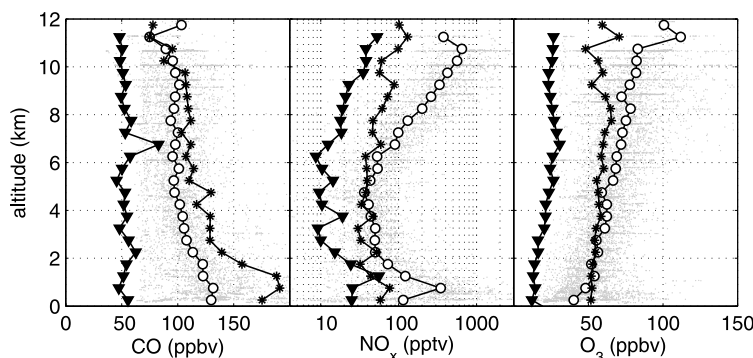


**Figure 6.** Comparisons of the median altitude profiles for atmospheric constituents in PEM Tropics B (triangles), TRACE-P (stars), and INTEX-A (circles) for (left) CO, (middle) NO<sub>x</sub>, and (right) O<sub>3</sub>. Individual 1-min measurements in INTEX-A are shown as gray points. For INTEX-A, NO<sub>x</sub> is the sum of measured NO<sub>2</sub> and calculated NO.



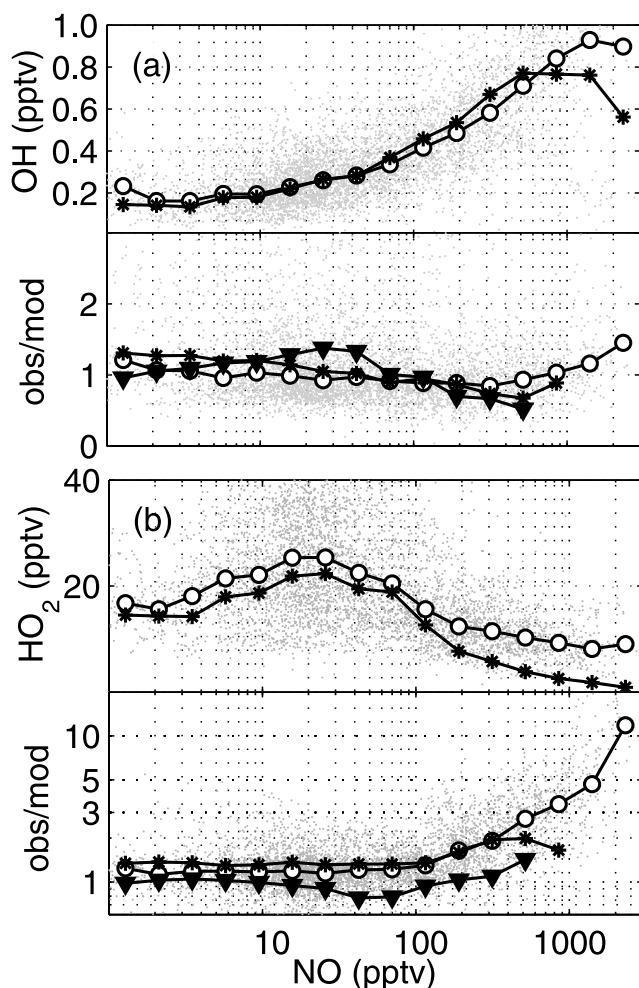


**Figure 7.** Comparison of NO dependence for (a) OH and (b) HO<sub>2</sub> of (top) measured (circles) and modeled (stars) values and (bottom) measured-to-modeled ratios in INTEX-A (circles), TRACE-P (stars) and PEM Tropics B (triangles). Individual INTEX-A 1-min measurements are shown (gray dots). Concentrations of NO calculated in the model are used. All lines show the median profiles.

However, unlike TRACE-P, where the observed-to-modeled ratio was around 1 in stratospherically influenced air, 92% of the INTEX-A observations with an observed-to-modeled HO<sub>2</sub> ratio significantly greater than 1 were in tropospheric air that was not obviously influenced by the stratosphere. Thus this INTEX-A result appears to be unprecedented.

[38] The behavior of the observed-to-modeled HO<sub>2</sub>/OH ratio is different in all three studies (Figure 5). For PEM-TB, the observed-to-modeled ratio near 1 at lower altitudes, but above 6 km begins to decrease, reaching 0.6 near 12 km. For TRACE-P, the opposite occurs; the ratio is slightly below 1 at low altitudes, but then increases to about 1.4 above 7 km. The INTEX-A observed-to-modeled HO<sub>2</sub>/OH ratios greater than 2 at altitudes above 8 km were not observed in the other studies. The large increase in the observed-to-modeled HO<sub>2</sub>/OH ratio at altitudes above 8 km is mainly driven by the underpredicted HO<sub>2</sub>.

### 3.2.2. Comparison as a Function of NO

[39] Both OH and HO<sub>2</sub> qualitatively show the expected behavior as a function of NO for INTEX-A (Figure 7), although important quantitative differences occur. For OH, the observed-to-modeled ratios for PEM-TB, TRACE-P, and INTEX-A are fairly constant with increasing NO.

[40] The observed-to-modeled HO<sub>2</sub> ratio increases from values below and near 1 to values more than 1 when NO is more than a few hundred pptv in all three studies, although the amount of change is different for the three studies. It is worth noting that the highest NO values were observed in the upper troposphere during INTEX-A, while the highest NO values were observed in boundary layer during TRACE-P.

### 3.3. HO<sub>x</sub> Budget Calculations

[41] Examining the HO<sub>x</sub> production and loss provides information about the balance between HO<sub>x</sub> sources and sinks. The HO<sub>x</sub> production consists of the production from the following processes: O<sub>3</sub> photolysis followed by the O(<sup>1</sup>D) + H<sub>2</sub>O reaction, HCHO photolysis (the radical-producing pathway only), H<sub>2</sub>O<sub>2</sub> photolysis, and the ozonolysis of alkenes. HO<sub>x</sub> loss includes the OH reaction with

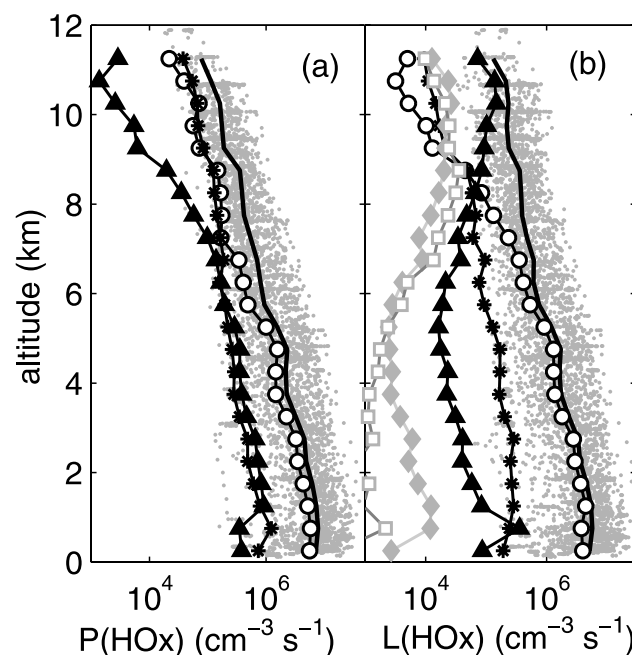


**Figure 8.** Vertical median profiles of (a) HO<sub>x</sub> production, showing total production (thick line) and production from O(<sup>1</sup>D) + H<sub>2</sub>O (circles), from HCHO photolysis (stars), and from H<sub>2</sub>O<sub>2</sub> photolysis (triangles), and (b) HO<sub>x</sub> loss rates, showing total loss rates (thick line) and loss rates due to HO<sub>2</sub> + HO<sub>2</sub>/RO<sub>2</sub> (circles), due to OH + HO<sub>2</sub> (stars), due to OH + NO<sub>x</sub> (triangles), due to OH + HNO<sub>3</sub> (diamonds), and due to OH + HO<sub>2</sub>NO<sub>2</sub> (squares) during INTEX-A. Small gray dots show the 1-min data for total HO<sub>x</sub> production rate (Figure 8a) and total HO<sub>x</sub> loss rate (Figure 8b). All the production and loss rates were calculated from the measurements, except for RO<sub>2</sub> + HO<sub>2</sub> where RO<sub>2</sub> levels were calculated in the model. The total production and loss rates are the sums of all production or loss terms.

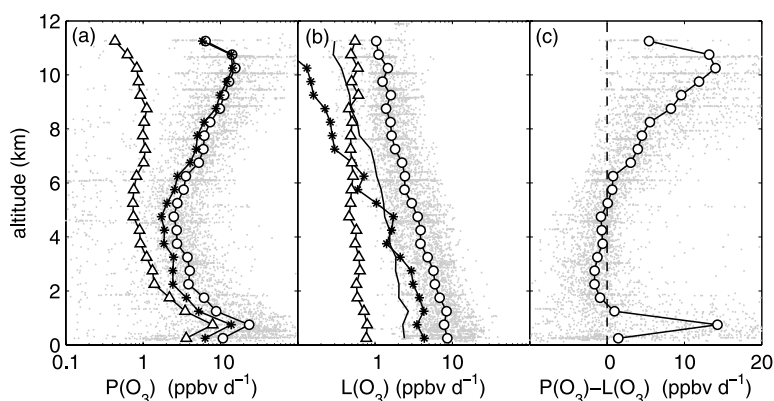


**Figure 9.** Vertical median profiles of (a) diurnal O<sub>3</sub> production rate, showing total production rates (circles) and production rates from HO<sub>2</sub> + NO (stars) and from RO<sub>2</sub> + NO (triangles) where RO<sub>2</sub> levels were calculated in the model; (b) O<sub>3</sub> loss rates, showing total loss rates (circles) and loss rates due to O(<sup>1</sup>D) + H<sub>2</sub>O (stars), due to O<sub>3</sub> + OH (triangles), and due to O<sub>3</sub> + HO<sub>2</sub> (solid line); and (c) net O<sub>3</sub> production rate during INTEX-A. Small gray dots show the 1-min data for total O<sub>3</sub> production rate (Figure 9a), total O<sub>3</sub> loss rate (Figure 9b), and net O<sub>3</sub> production (Figure 9c).

NO<sub>2</sub> and the reactions among OH, HO<sub>2</sub> and RO<sub>2</sub>. For this discussion, RO<sub>2</sub> was calculated by the box model.

[42] The main P(HO<sub>x</sub>) was the reaction O(<sup>1</sup>D) + H<sub>2</sub>O below 7 km and the photolysis of HCHO above 7 km (Figure 8a). Photolysis of H<sub>2</sub>O<sub>2</sub> contributed little to P(HO<sub>x</sub>). For the HO<sub>x</sub> loss, HO<sub>2</sub>-RO<sub>2</sub> self-reactions were the main processes below 8 km and the OH + NO<sub>x</sub> reactions became the main loss processes above 8 km (Figure 8b).

### 3.4. Diurnal Average of Calculated Ozone Production

[43] The net calculated ozone production in the troposphere is given to a close approximation by

$$\begin{aligned}
 P(\text{O}_3)_{\text{net}} = P(\text{O}_3) - L(\text{O}_3) = & k_{\text{NO}+\text{HO}_2}[\text{NO}][\text{HO}_2] \\
 & + \sum_i k_{\text{NO}+\text{RO}_{2i}}[\text{NO}][\text{RO}_{2i}] - k_{\text{OH}+\text{NO}_2+\text{M}}[\text{M}][\text{NO}_2][\text{OH}] \\
 & - k_{\text{O}(\text{D})+\text{H}_2\text{O}}[\text{O}(\text{D})][\text{H}_2\text{O}] - k_{\text{HO}_2+\text{O}_3}[\text{O}_3][\text{HO}_2] \\
 & - k_{\text{OH}+\text{O}_3}[\text{O}_3][\text{OH}]
 \end{aligned} \quad (2)$$

where  $k_{\text{NO}+\text{HO}_2}$ ,  $k_{\text{NO}+\text{RO}_{2i}}$ ,  $k_{\text{OH}+\text{NO}_2+\text{M}}$ ,  $k_{\text{O}(\text{D})+\text{H}_2\text{O}}$ ,  $k_{\text{HO}_2+\text{O}_3}$ , and  $k_{\text{OH}+\text{O}_3}$  are reaction rate coefficients. The diurnally averaged values of the calculated ozone production and loss terms come from the time-dependent model simulations. In order to determine the O<sub>3</sub> budget based on observed values of HO<sub>x</sub>, the model was run with the computed diurnal profiles of OH and HO<sub>2</sub> scaled throughout the diurnal cycle to match the observed concentrations at the appropriate time of day. The resulting calculated O<sub>3</sub> production was mainly from the HO<sub>2</sub> + NO reaction, especially at altitudes greater than 5 km (Figure 9a). At altitudes around 10 km, the calculated O<sub>3</sub> production from RO<sub>2</sub> + NO accounted for less than 10% of the total. For the O<sub>3</sub> loss rate, O<sub>3</sub> photolysis followed by the O(<sup>1</sup>D) + H<sub>2</sub>O reaction was the main O<sub>3</sub> loss process below 5 km, while O<sub>3</sub> reactions with OH and HO<sub>2</sub> became the main O<sub>3</sub> loss above 6 km because of low H<sub>2</sub>O mixing ratios at these altitudes (Figure 9b).

[44] Net calculated ozone production with a median value of 8.4 ppbv d<sup>-1</sup> was found for the lowest altitude (<1 km), while a median loss of 0.8 ppbv d<sup>-1</sup> was found for the lower troposphere (1–5 km). For observations above 9 km, a

median net O<sub>3</sub> production rate of 11.4 ppbv d<sup>-1</sup> was calculated (Figure 9c). For the upper altitudes, the O<sub>3</sub> production drops to 4.5 ppbv d<sup>-1</sup> when model predictions of HO<sub>x</sub> are used rather than observed values. This significant difference underscores the importance of understanding the upper tropospheric HO<sub>x</sub> discrepancies in the INTEX-A data. The important role of lightning NO<sub>x</sub> is also emphasized by the large rates of net production in INTEX-A compared to previous campaigns. Calculated ozone production in the upper troposphere during TRACE-P was less than 1.5 ppbv d<sup>-1</sup> [Davis *et al.*, 2003] and was ~0.5 ppbv d<sup>-1</sup> during PEM-Tropics B [Olson *et al.*, 2001].

## 4. Discussion

[45] Two significant differences between observed and modeled HO<sub>x</sub> become apparent in the INTEX-A data: underpredicted HO<sub>2</sub> above 8 km and underpredicted OH in the continental planetary boundary layer.

### 4.1. Underpredicted HO<sub>2</sub> Above 8 km Altitude

[46] Convection had a large impact on the atmospheric composition in this altitude range during INTEX-A [Bertram *et al.*, 2007], most notably with enhancements for lightning NO<sub>x</sub> (Figure 6), but also for peroxides, HCHO, and sometimes other constituents. Above 8 km, more than 2/3 of the observations of HO<sub>2</sub> and HO<sub>2</sub>/OH were greater than expected, while only a small number of OH observations were.

[47] Could this underpredicted HO<sub>2</sub> be an instrument artifact? An offset to the HO<sub>2</sub> signal would make HO<sub>2</sub> appear larger than it is. However, the observed-to-modeled HO<sub>2</sub> ratio is uncorrelated with observed HO<sub>2</sub>, which varied from 3 pptv to 30 pptv above 8 km. In addition, no single offset HO<sub>2</sub> value can be found to improve the agreement between the observed and modeled HO<sub>2</sub>. These results rule out a constant offset in the HO<sub>2</sub> signal. The only gas that is known to photolyze in the ATHOS laser beam to produce HO<sub>2</sub>, but no OH, is formaldehyde, but the HCHO measured

in INTEX-A is orders of magnitude too small to produce the observed signals [Ren *et al.*, 2004].

[48] The large observed-to-modeled HO<sub>2</sub> ratio above 8 km is consistent with the underpredicted H<sub>2</sub>O<sub>2</sub>, but not consistent with observed pernitric acid (HO<sub>2</sub>NO<sub>2</sub>). If HO<sub>2</sub>NO<sub>2</sub> were in steady state with HO<sub>2</sub> and NO<sub>2</sub>, the calculated steady state value of HO<sub>2</sub> would need to be lower than even the modeled HO<sub>2</sub>. This difference is consistent with the possibility of the termination reaction for OH that actually improves the model-to-observed comparison for HO<sub>2</sub>NO<sub>2</sub> [Kim *et al.*, 2007].

[49] If the observed HO<sub>2</sub> is not an instrument artifact, then the underpredicted HO<sub>2</sub> indicates an additional unknown HO<sub>x</sub> source or a reduced HO<sub>x</sub> sink; the underpredicted HO<sub>2</sub>/OH indicates either slower HO<sub>x</sub> cycling from HO<sub>2</sub> to OH or faster HO<sub>x</sub> cycling from OH to HO<sub>2</sub>.

[50] Consider first the underprediction of HO<sub>2</sub>. Either an additional unknown HO<sub>x</sub> source or a reduced HO<sub>x</sub> sink must be capable of improving the observed-to-modeled HO<sub>2</sub> agreement above 8 km without making the agreement worse at lower altitudes. Thus, the cause of HO<sub>2</sub> underprediction must be insignificant from 2 to 8 km and must have increasing importance from 8 to 11 km.

[51] If a reduced HO<sub>x</sub> sink is the cause, then the error would need to be in the known termination reactions of OH with NO<sub>2</sub>, NO, HNO<sub>3</sub>, and HO<sub>2</sub>NO<sub>2</sub> because they dominate above 8 km and are insignificant below 8 km (Figure 8). However, for terminal HO<sub>x</sub> loss by reaction with NO<sub>x</sub> to be the cause of the HO<sub>2</sub> underprediction, the HO<sub>x</sub> loss rate by these reactions would have to be 5 to 8 times less than expected. This difference is well outside uncertainties for the measured reactants and reaction rate coefficients. Thus, a reduced HO<sub>x</sub> sink is unlikely to be the cause of the HO<sub>2</sub> underprediction.

[52] If underpredicted HO<sub>x</sub> production is the cause, then the error would need to result from either an error in the known HO<sub>x</sub> sources or additional unknown HO<sub>x</sub> sources. The known, equally dominant HO<sub>x</sub> sources in the altitude region are O<sub>3</sub> photolysis followed by O(<sup>1</sup>D) + H<sub>2</sub>O and HCHO photolysis. In order to bring modeled and observed HO<sub>2</sub> into agreement, an additional HO<sub>x</sub> source of  $1.5 \times 10^6$  molecules cm<sup>-3</sup> s<sup>-1</sup> is needed above 8 km. This amount is about 4 times larger than the known HO<sub>x</sub> sources (Figure 8). Below 8 km, this source would need to decrease to less than  $\sim 10^5$  molecules cm<sup>-3</sup> s<sup>-1</sup> at 6 km and below. It is worth noting that this increase with altitude of the needed additional HO<sub>x</sub> source is similar to the observed increase in NO<sub>x</sub> with increasing altitude (Figure 6).

[53] Can the HO<sub>2</sub> underprediction come from errors in a known source? The O<sub>3</sub> photolysis and HCHO photolysis are about equal HO<sub>x</sub> sources above 8 km. The HO<sub>x</sub> production rate from either one of them would need to be increased by a factor of 4 to 6 above 10 km. O<sub>3</sub> photolysis could not be low by that much at 10 km and still be consistent with the HO<sub>x</sub> observed-to-modeled ratios below 10 km, where O<sub>3</sub> photolysis is the dominant HO<sub>x</sub> source. This inconsistency rules out an error in O<sub>3</sub> photolysis as the cause of the HO<sub>2</sub> underprediction. Constraining the model to observed HCHO reduces the observed-to-modeled HO<sub>2</sub> ratio by less than 25% (Fried *et al.*, submitted manuscript, 2007). The HCHO photolysis frequency is unlikely to be in error by the factor of 4 to 6 needed to bring the measured and modeled

HO<sub>2</sub> into agreement, because there is good agreement between the photolysis frequency measurements and radiative transfer model results at all altitudes. It is important to note that the Fried *et al.* (submitted manuscript, 2007) study also observed a HCHO measurement/model discrepancy between 10 km and 12 km that scaled with NO, similar to the HO<sub>2</sub> discrepancy.

[54] Thus, unknown HO<sub>x</sub> sources are the most likely cause of the HO<sub>2</sub> underprediction. One characteristic of the unknown source is that it correlates with NO. For the observed-to-modeled HO<sub>2</sub> ratio above 8 km, the HO<sub>2</sub> observed-to-modeled ratio =  $0.004 \times \text{NO}$  (in pptv) + 0.88 with  $r^2 = 0.54$ . In previous studies, it was assumed that the chemistry and HO<sub>x</sub> sinks were understood and that the underpredicted HO<sub>2</sub> was due to missing HO<sub>x</sub> sources that were emitted along with the NO [see, e.g., Folkins *et al.*, 1997; Wennberg *et al.*, 1998; Jaeglé *et al.*, 2000]. While we have been able to quantify the additional HO<sub>x</sub> production that would be needed, to identify its altitude dependence, and to show a correlation with NO, we have not been able to identify this additional unknown HO<sub>x</sub> source.

[55] A second issue is the underpredicted HO<sub>2</sub>/OH ratio. This ratio indicates that reactions and reactants that cycle HO<sub>x</sub> between OH and HO<sub>2</sub> are not being properly represented in the model. The HO<sub>2</sub>/OH underprediction can be explained by either slower reactions of HO<sub>2</sub> with NO or faster OH reactions that cycle OH to HO<sub>2</sub>. At these altitudes, the reaction frequency of HO<sub>2</sub> + NO → OH + NO<sub>2</sub> is an order of magnitude faster than primary OH production (equation (1)). The reaction frequency for HO<sub>2</sub> + NO would need to be less than  $\frac{1}{2}$  its calculated value; this difference is unlikely and inconsistent with many other studies. It is possible that other reactants with HO<sub>2</sub>, such as BrO, are present, but their reactions with HO<sub>2</sub> would make HO<sub>2</sub>/OH smaller, not larger. Thus, the underpredicted HO<sub>2</sub>/OH ratio indicates the presence of unknown reactants or reactions with OH that cycle HO<sub>x</sub> from OH to HO<sub>2</sub>.

[56] In this case, the needed increase in the OH reactivity that cycles HO<sub>x</sub> between OH and HO<sub>2</sub> is proportional to the observed-to-modeled HO<sub>2</sub>/OH ratio. As a result, the needed additional OH reactivity is  $\sim 0.15$  s<sup>-1</sup> at 8 km, about  $\frac{1}{2}$  of the calculated OH reactivity, and  $\sim 0.5$  s<sup>-1</sup> above 10 km, almost twice the calculated OH reactivity. Interestingly, the needed OH reactivity is roughly proportional to the increase in NO<sub>x</sub> in that altitude range, suggesting that the convective processes that enhanced NO<sub>x</sub> also yielded additional, unknown OH reactants.

[57] In the presence of greater NO, the differences in OH and HO<sub>2</sub> between the model constrained to observed H<sub>2</sub>O<sub>2</sub>, CH<sub>3</sub>OOH, HNO<sub>3</sub>, and PAN and the model unconstrained by these observations grows (Figure 10). This behavior indicates that the modeled OH and HO<sub>2</sub> are quite sensitive to the model constraints, especially above 8 km altitude where the NO was increasing. In this altitude region, the cycling of HO<sub>2</sub> due to NO dominates the production of OH and makes HO<sub>x</sub> more sensitive to small differences in the constraints placed on the model photochemistry.

#### 4.2. Underpredicted OH in the Continental Planetary Boundary Layer

[58] During INTEX-A, the observed-to-modeled OH ratio is frequently much greater than 1.0 below 2 km altitude in



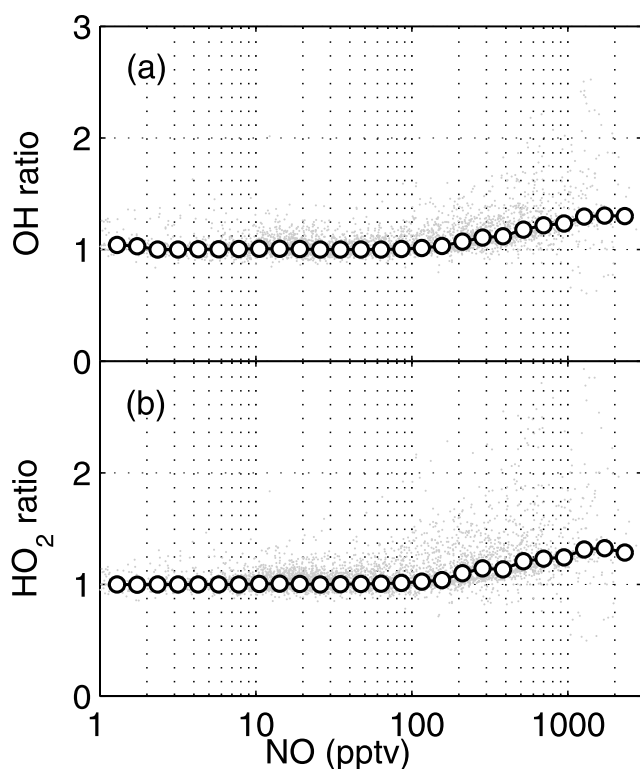


**Figure 10.** Ratio of constrained-to-unconstrained models for (a) OH and (b) HO<sub>2</sub> as a function of NO. Individual 1-min comparisons are presented (gray dots) as well as median values (circles and lines).

the planetary boundary layer. The location of these large ratios coincides with forested regions where isoprene is abundant, primarily from the Gulf Coast states up through Appalachia and the Midwest. The observed-to-modeled OH ratio is a strong function of isoprene (Figure 11). It increases slowly from 1.0 to 1.5 as isoprene increases from less than 10 pptv to 500 pptv, but for isoprene levels exceeding 500 pptv, the observed-to-modeled OH ratio rapidly increased to  $\sim 5$  as isoprene increases. The observed and

modeled OH levels diverge for isoprene levels greater than 100 pptv (Figure 11). This underprediction of OH is consistent with the underprediction of HO<sub>2</sub> below 2 km altitude. As shown in Table 1, 56% of the measured HO<sub>2</sub> is greater than the modeled HO<sub>2</sub> times 1.32.

[59] This observation from INTEX-A is consistent with tower-based observations made with a different configuration of the same instrument. In the summers of 1998 and 2000, OH and isoprene measurements were made on a tower at the PROPHET site in a Michigan forest [Tan *et al.*, 2001b]. The median daytime (SZA < 60°) observed-to-modeled OH ratio depends on isoprene in a way that is consistent with and overlaps the INTEX-A measurements (Figure 11).

[60] The reasons for the higher-than-expected OH at high isoprene levels are not clear, but most likely are due to a missing OH source in the model. For PROPHET, the agreement between observed and modeled OH is improved by introducing additional terpenes that react with O<sub>3</sub> to form OH [Tan *et al.*, 2001b]. In addition, the difference between the observed and calculated OH reactivity is consistent with the emissions of unmeasured terpene such as terpinolene in terms of its reaction rate with O<sub>3</sub> to that with OH and OH yield in the O<sub>3</sub> reaction [Di Carlo *et al.*, 2004]. The missing OH source can also be the OH production in the HO<sub>2</sub> reactions with certain RO<sub>2</sub>, in which a significant OH yield was suggested by Hasson *et al.* [2004]. An error in our understanding of the rate coefficients or products of these kinds of reactions might cause models to predict too little OH [Thornton *et al.*, 2002], though our initial model analysis could not reconcile the missing OH source with this feedback. Another possible missing OH source over forests is the photolysis of HONO [Zhou *et al.*, 2002; Kleffmann *et al.*, 2005; Stemmler *et al.*, 2006]. While the OH was severely underpredicted in PROPHET by a model that included HONO measurements, for INTEX-A, the possible contribution of HONO to the missing OH source cannot be ruled out because no HONO measurements were made on the NASA DC-8. That the underpredicted OH was observed over several forested areas during INTEX-A provides strong evidence that this effect is not specific only to the PROPHET site in northern lower Michigan, but is, in

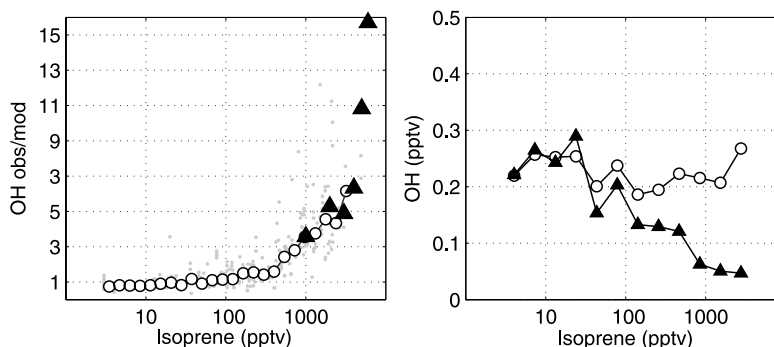


**Figure 11.** (left) The observed-to-modeled OH ratio as a function of isoprene. Individual 1-min measurements (gray points) and median values for isoprene intervals (circles) are shown for data taken at less than 1 km altitude and solar zenith angle less than 60°. Median observed-to-modeled OH ratios from the PROPHET tower in a Michigan forest in summer 2000 are also shown (triangles). (right) The median observed OH (circles) and modeled OH (triangles) as a function of isoprene.



fact, a more widespread property of atmospheric chemistry over forests.

## 5. Summary and Conclusions

[61] Measurements of OH and HO<sub>2</sub> were compared to the model calculations in the INTEX-A summer 2004 campaign. This study provides an excellent opportunity to test oxidation chemistry throughout the troposphere. The following conclusions can be drawn from this study.

[62] First, for most of the troposphere, observed OH and HO<sub>2</sub> agree well with model calculations. On average observed OH was 0.95 of modeled OH and observed HO<sub>2</sub> was 1.28 of modeled HO<sub>2</sub>. This observed-to-modeled comparison is similar to that for TRACE-P, another midlatitude study for which the median observed-to-modeled ratio was 1.08 for OH and 1.34 for HO<sub>2</sub>, and to that for PEM-TB, a tropical study for which the median observed-to-modeled ratio was 1.17 for OH and 0.97 for HO<sub>2</sub>. In contrast, above 8 km during INTEX-A, the median observed-to-modeled HO<sub>2</sub> ratio increased from about 1.2 at 8 km to about 3 at 11 km.

[63] Second, an HO<sub>x</sub> budget analysis shows that the main HO<sub>x</sub> sources are O<sub>3</sub> photolysis followed by the O(<sup>1</sup>D) + H<sub>2</sub>O reaction below 7 km and the photolysis of HCHO above 7 km. The main HO<sub>x</sub> sinks are the HO<sub>2</sub>-RO<sub>2</sub> self-reactions below 8 km and OH + NO<sub>x</sub> reactions above 8 km.

[64] Third, an O<sub>3</sub> budget analysis shows that the diurnally averaged net calculated O<sub>3</sub> loss rate was 0.8 ppbv d<sup>-1</sup> at altitudes between 1 and 5 km. Above 9 km, the diurnally averaged net calculated O<sub>3</sub> production rate was 4.5 ppbv d<sup>-1</sup> using modeled HO<sub>2</sub> and 11.4 ppbv d<sup>-1</sup> using observed HO<sub>2</sub>. This difference between the net calculated O<sub>3</sub> production from the modeled HO<sub>2</sub> and the observed HO<sub>2</sub> is significant and a concern.

[65] Fourth, the underpredicted HO<sub>2</sub> at altitudes above 8 km suggests the presence of an unknown HO<sub>x</sub> source or an error in the model's chemistry involving some of the other atmospheric constituents. The concurrent increases of the observed-to-modeled HO<sub>2</sub> ratio and NO with altitude suggest that an unknown HO<sub>x</sub> source comes from the convective processes that cause the enhanced NO. Evidence from the constrained and unconstrained model runs indicates that model predictions of OH and HO<sub>2</sub> are particularly sensitive to the NO.

[66] Fifth, the observed-to-modeled OH ratio in the planetary boundary layer in forested regions is a strong function of isoprene. It increases slowly from 1.0 to 1.5 as isoprene increases from less than 10 pptv to 500 pptv, but for isoprene levels exceeding 500 pptv, the observed-to-modeled OH ratio rapidly increased to ~5. This isoprene dependence of observed-to-modeled OH ratio is consistent with the PROPHET measurements, indicating that this underpredicted OH, if not due to instrument artifacts, occurs in widespread forested regions.

[67] It seems more likely to us that the causes of underpredicted HO<sub>2</sub> above 8 km are due to unknown atmospheric constituents that are acting as HO<sub>x</sub> sources or OH sinks or to unknown reactions and not to large errors in the measurements of either atmospheric constituents or the photochemical rate coefficients. These two major differences between observed and modeled HO<sub>x</sub>, underpredicted HO<sub>2</sub> above

8 km and underpredicted OH in the planetary boundary layer in forested regions, appear to have different causes.

[68] Because the underpredicted HO<sub>2</sub> above 8 km and underpredicted OH above forests have strong implications for understanding global-scale tropospheric oxidation chemistry, finding the causes for these differences should be a high priority. Progress in resolving these discrepancies requires a focused research activity devoted to further examination of possible unknown OH sinks and HO<sub>x</sub> sources.

[69] **Acknowledgments.** The work was supported by the NASA Tropospheric Chemistry Program. The authors would like to thank the DC-8 crew and support staff during the INTEX-A preparation and deployment periods for making this work possible.

## References

- Bertram, T. H., et al. (2007), Direct measurement of the convective recycling of the upper troposphere, *Science*, **315**, 816–820, doi:10.1126/science.1134548.
- Bloss, W. J., J. D. Lee, D. E. Heard, R. A. Salmon, S. J.-B. Bauguitte, H. K. Roscoe, and A. E. Jones (2007), Observations of OH and HO<sub>2</sub> radicals in coastal Antarctica, *Atmos. Chem. Phys.*, **7**, 4171–4185.
- Brune, W. H., et al. (1998), Airborne in-situ OH and HO<sub>2</sub> observations in the cloud-free troposphere and lower stratosphere during SUCCESS, *Geophys. Res. Lett.*, **25**, 1701–1704.
- Brune, W. H., et al. (1999), OH and HO<sub>2</sub> chemistry in the North Atlantic free troposphere, *Geophys. Res. Lett.*, **26**, 3077–3080.
- Carlsaw, N., P. J. Jacobs, and M. J. Pilling (1999), Modeling OH, HO<sub>2</sub>, and RO<sub>2</sub> radicals in the marine boundary layer: 2. Mechanism reduction and uncertainty analysis, *J. Geophys. Res.*, **104**, 30,257–30,273.
- Crawford, J., et al. (1999), Assessment of upper tropospheric HO<sub>x</sub> source over the tropical Pacific based on NASA GTE/PEM data: Net effect on HO<sub>x</sub> and other photochemical parameters, *J. Geophys. Res.*, **104**, 16,255–16,273.
- Davis, D. D., et al. (2003), An assessment of western North Pacific ozone photochemistry based on springtime observations from NASA's PEM-West B (1994) and TRACE-P (2001) field studies, *J. Geophys. Res.*, **108**(D21), 8829, doi:10.1029/2002JD003232.
- Di Carlo, P., et al. (2004), Missing OH reactivity in a forest: evidence for unknown reactive biogenic VOCs, *Science*, **304**, 722–725.
- Eisele, F. L., et al. (2001), Relationship between OH measurements on two different NASA aircraft during PEM Tropics B, *J. Geophys. Res.*, **106**, 32,683–32,689.
- Eisele, F. L., et al. (2003), Summary of measurement intercomparisons during TRACE-P, *J. Geophys. Res.*, **108**(D20), 8791, doi:10.1029/2002JD003167.
- Faloona, I. C., et al. (2004), A laser-induced fluorescence instrument for detecting tropospheric OH and HO<sub>2</sub>: Characteristics and calibration, *J. Atmos. Chem.*, **47**, 139–167.
- Folkens, I., P. O. Wennberg, T. F. Hanisco, J. G. Anderson, and R. J. Salawitch (1997), OH, HO<sub>2</sub>, and NO in two biomass burning plumes: Sources of HO<sub>x</sub> and implications for ozone production, *Geophys. Res. Lett.*, **24**, 3185–3188.
- Hanisco, T. F., J. B. Smith, R. M. Stimpfle, D. M. Wilmouth, J. G. Anderson, E. C. Richard, and T. P. Bui (2002), In situ observations of HO<sub>2</sub> and OH obtained on the NASA ER-2 in the high-CIO conditions of the 1999/2000 Arctic polar vortex, *J. Geophys. Res.*, **107**(D20), 8283, doi:10.1029/2001JD001024.
- Hard, T. M., R. J. O'Brien, C. Y. Chan, and A. A. Mehrabzadeh (1984), Tropospheric free radical determination by FAGE, *Environ. Sci. Technol.*, **18**, 768–777.
- Hasson, A. S., G. S. Tyndall, and J. J. Orlando (2004), A product yield study of the reaction of HO<sub>2</sub> radicals with ethyl peroxy (C<sub>2</sub>H<sub>5</sub>O<sub>2</sub>), acetyl peroxy (CH<sub>3</sub>C(O)O<sub>2</sub>), and acetyl peroxy (CH<sub>3</sub>C(O)CH<sub>2</sub>O<sub>2</sub>) radicals, *J. Phys. Chem. A*, **108**, 5979–5989.
- Jacob, D. J., J. H. Crawford, M. M. Kleb, V. S. Connors, R. J. Bendura, J. L. Raper, G. W. Sachse, J. C. Gille, L. Emmons, and C. L. Heald (2003), Transport and Chemical Evolution over the Pacific (TRACE-P) aircraft mission: Design, execution, and first results, *J. Geophys. Res.*, **108**(D20), 9000, doi:10.1029/2002JD003276.
- Jaeglé, L., et al. (2000), Photochemistry of HO<sub>x</sub> in the upper troposphere at northern midlatitudes, *J. Geophys. Res.*, **105**, 3877–3892.
- Jaeglé, L., D. J. Jacob, W. H. Brune, and P. O. Wennberg (2001), Chemistry of HO<sub>x</sub> radicals in the upper troposphere, *Atmos. Environ.*, **35**, 469–489.

- Kim, S., et al. (2007), Measurement of HO<sub>2</sub>NO<sub>2</sub> in the free troposphere during the Intercontinental Chemical Transport Experiment–North America 2004, *J. Geophys. Res.*, **112**, D12S01, doi:10.1029/2006JD007676.
- Kleffmann, J., T. Gavriloaiei, A. Hofzumahaus, F. Holland, R. Koppmann, L. Rupp, E. Schlosser, M. Siese, and A. Wahner (2005), Daytime formation of nitrous acid: A major source of OH radicals in a forest, *Geophys. Res. Lett.*, **32**, L05818, doi:10.1029/2005GL022524.
- Kleinman, L. I., P. H. Daum, Y. Lee, L. J. Nunnermacker, S. R. Springston, J. Weinstein-Lloyd, and J. Rudolph (2002), Ozone production efficiency in an urban area, *J. Geophys. Res.*, **107**(D23), 4733, doi:10.1029/2002JD002529.
- Madronich, S., and S. Flocke (1998), The role of solar radiation in atmospheric chemistry, in *Handbook of Environmental Chemistry*, edited by P. Boule, pp. 1–26, Springer, New York.
- McKeen, S. A., et al. (1997), Photochemical modeling of hydroxyl and its relationship to other species during the Tropospheric OH Photochemistry Experiment, *J. Geophys. Res.*, **102**, 6467–6493.
- Murphy, J. G., J. A. Thornton, P. J. Wooldridge, D. A. Day, R. S. Rosen, C. Cantrell, R. E. Shetter, B. Lefer, and R. C. Cohen (2004), Measurements of the sum of HO<sub>2</sub>NO<sub>2</sub> and CH<sub>3</sub>O<sub>2</sub>NO<sub>2</sub> in the remote troposphere, *Atmos. Chem. Phys.*, **4**, 377–384.
- Olson, J. R., et al. (2001), Seasonal differences in the photochemistry of the South Pacific: A comparison of observations and the model results from PEM-Tropics A and B, *J. Geophys. Res.*, **106**, 32,749–32,766.
- Olson, J. R., et al. (2004), Testing fast photochemical theory during TRACE-P based on measurements of OH, HO<sub>2</sub>, and CH<sub>2</sub>O, *J. Geophys. Res.*, **109**, D15S10, doi:10.1029/2003JD004278.
- Olson, J. R., J. H. Crawford, G. Chen, W. H. Brune, I. C. Faloona, D. Tan, H. Harder, and M. Martinez (2006), A reevaluation of airborne HO<sub>x</sub> observations from NASA field campaigns, *J. Geophys. Res.*, **111**, D10301, doi:10.1029/2005JD006617.
- Raper, J. L., et al. (2001), Pacific Exploratory Mission in the Tropical Pacific: PEM-Tropics B, March–April 1999, *J. Geophys. Res.*, **106**, 32,401–32,425.
- Ren, X., G. D. Edwards, C. A. Cantrell, R. L. Leshner, A. R. Metcalf, T. Shirley, and W. H. Brune (2003), Intercomparison of peroxy radical measurements at a rural site using laser-induced fluorescence and Peroxy Radical Chemical Ionization Mass Spectrometer (PerCIMS) techniques, *J. Geophys. Res.*, **108**(D19), 4605, doi:10.1029/2003JD003644.
- Ren, X., H. Harder, M. Martinez, I. Faloona, D. Tan, R. L. Leshner, P. Di Carlo, J. B. Simpas, and W. H. Brune (2004), Interference testing for atmospheric HO<sub>x</sub> measurements by laser-induced fluorescence, *J. Atmos. Chem.*, **47**, 169–190.
- Shetter, R. E., and M. Muller (1999), Photolysis frequency measurements using actinic flux spectroradiometry during the PEM-Tropics mission: Instrumentation description and some results, *J. Geophys. Res.*, **104**, 5647–5661.
- Singh, H. B., M. Kandaidou, P. J. Crutzen, and D. J. Jacob (1995), High concentrations and photochemical fate of oxygenated hydrocarbons in the global troposphere, *Nature*, **378**, 50–54.
- Singh, H. B., W. H. Brune, and J. H. Crawford (2003), Reactive nitrogen and hydrogen in the global atmosphere: Progress in measurements and theory, in *Recent Advances in Atmospheric and Oceanic Sciences—Part II: Air Pollution Studies*, *Proc. Indian Natl. Sci. Acad.*, **69**(6), 669–683.
- Singh, H. B., W. H. Brune, J. H. Crawford, D. J. Jacob, and P. B. Russell (2006), Overview of the Summer 2004 Intercontinental Chemical Transport Experiment–North America (INTEx-A), *J. Geophys. Res.*, **111**, D24S01, doi:10.1029/2006JD007905.
- Stemmler, K., M. Ammann, C. Donders, J. Kleffmann, and C. George (2006), Photosensitized reduction of nitrogen dioxide on humic acid as a source of nitrous acid, *Nature*, **440**, 195–198, doi:10.1038/nature04603.
- Tan, D., et al. (2001a), OH and HO<sub>2</sub> in the tropical Pacific: Results from PEM Tropics B, *J. Geophys. Res.*, **106**, 32,667–32,681.
- Tan, D., et al. (2001b), HO<sub>x</sub> budgets in a deciduous forest: Results from the PROPHET summer 1998 campaign, *J. Geophys. Res.*, **106**, 24,407–24,427.
- Thompson, A. M., and R. W. Stewart (1991), Effect of chemical kinetics uncertainties on calculated constituents in a tropospheric photochemical model, *J. Geophys. Res.*, **96**, 13,089–13,108.
- Thornton, J. A., P. J. Wooldridge, and R. C. Cohen (2000), Atmospheric NO<sub>2</sub>: In situ laser-induced fluorescence detection at parts per trillion mixing ratios, *Anal. Chem.*, **72**, 528–539.
- Thornton, J. A., et al. (2002), Ozone production rates as a function of NO<sub>x</sub> abundances and HO<sub>x</sub> production rates in the Nashville urban plume, *J. Geophys. Res.*, **107**(D12), 4146, doi:10.1029/2001JD000932.
- Wennberg, P. O., et al. (1998), Hydrogen radicals, nitrogen radicals, and the production of O<sub>3</sub> on the upper troposphere, *Science*, **279**, 49–53.
- Zhou, X., K. Civerolo, H. Dai, G. Huang, J. Schwab, and K. Demerjian (2002), Summertime nitrous acid chemistry in the atmospheric boundary layer at a rural site in New York State, *J. Geophys. Res.*, **107**(D21), 4590, doi:10.1029/2001JD001539.
- M. A. Avery, J. D. Barrick, G. Chen, J. H. Crawford, J. R. Olson, G. W. Sachse, and G. S. Diskin, Science Directorate, NASA Langley Research Center, Hampton, VA 23681, USA.
- D. R. Blake, Department of Chemistry, University of California, Irvine, CA 92697, USA.
- W. H. Brune, Z. Chen, R. B. Long, and J. Mao, Department of Meteorology, Pennsylvania State University, University Park, PA 16802, USA.
- R. C. Cohen, Department of Chemistry, University of California, Berkeley, CA 94720, USA.
- A. Fried, Earth Observing Laboratory, National Center for Atmospheric Research, Boulder, CO 80307, USA.
- B. Heikes, Graduate School of Oceanography, University of Rhode Island, Narragansett, RI 02881, USA.
- L. G. Huey, School of Earth and Atmospheric Sciences, Georgia Institute of Technology, Atlanta, GA 30332, USA.
- X. Ren, Rosenstiel School of Marine and Atmospheric Sciences, University of Miami, Miami, FL 33149, USA. (xren@rsmas.miami.edu)
- H. B. Singh, NASA Ames Research Center, Moffett Field, CA 94035, USA.
- R. E. Shetter, National Suborbital Education and Research Center, University of North Dakota, Grand Forks, ND 58202, USA.
- P. O. Wennberg, Division of Engineering and Applied Sciences, California Institute of Technology, Pasadena, CA 91125, USA.